Pure spin current-induced domain wall motion probed by localized spin signal detection

Nils Motzko,[1] Björn Burkhardt,[1] Nils Richter,[1] Robert Reeve,[1] Piotr Laczkowski,[2] Williams Savero Torres,[2] Laurent Vila,[2] Jean-Philippe Attané,[2,3] and Mathias Kläui[1,*]

[1]*Institut für Physik, Johannes Gutenberg-Universität Mainz, 55099 Mainz, Germany*

[2]*INAC, CEA Grenoble, 17 avenue des Martyrs, 38054 Grenoble, France*

[3]*Universite Joseph Fourier, BP 53, 38041 Grenoble, France*

(Received 28 September 2013; published 10 December 2013)

We demonstrate the displacement of domain walls via pure diffusive spin currents in a nonlocal spin valve geometry, without any externally applied fields. We implement a localized detection of the domain wall position by simultaneous nonlocal spin signal measurements using contacts on both sides of the spin current conduit, which allows us to determine the domain wall position even underneath the spin current conduit. Using this detection method, we probe the domain wall position as it moves across the spin current conduit when sweeping a field or on current application. Injecting pure spin currents in the nonlocal architecture, we find that in our optimized geometry we can displace a transverse head-to-head or tail-to-tail domain wall without any externally applied fields at effective spin currents $<10^{10}$ A/m^2, showing that this method can be a viable avenue to low-power domain wall manipulation.

DOI: 10.1103/PhysRevB.88.214405 PACS number(s): 72.25.−b, 75.60.Ch

The manipulation of magnetization using spin currents currently receives significant interest due to the fundamental interaction of spin currents with magnetization that leads to spin transfer torques and, on the application side, due to the favorable scaling of this approach for devices in terms of energy requirements.[1] The now well-established spin transfer torque using spin-polarized charge currents was predicted some time ago,[2,3] and was more recently experimentally shown to be able to displace spin structures such as domain walls[4–6] using charge currents that become spin polarized in the magnetic material. For the spin torque effect, however, one is only interested in the spin current with the charge current only leading to unwanted ohmic losses and resulting Joule heating, which can disturb the spin structure due to heating of the material close to its Curie temperature.[7] So approaches that reduce the Joule heating have been sought and, in recent years, the focus has shifted to pure diffusive spin currents without net charge currents flowing. While this still entails a certain amount of Joule heating during the spin current generation, no net charge current flows at the position of the domain wall and thus the heating at the domain wall position is reduced. In general, to use such diffusive spin currents, they need to be first generated in a spin current source, transported, for instance, in a nonmagnetic spin current conduit and eventually used to manipulate magnetization. The magnetization acts as a spin current sink, absorbing the spin current, which reciprocally leads to the exertion of a torque on the magnetization. There are various ways to generate such spin currents. Sources include the spin Hall effect, where a spin accumulation is generated at the surfaces of materials with large spin-orbit coupling, and this can then be injected into a spin current conduit that carries the spin current.[8] Dynamic spin pumping can inject pure spin currents from ferromagnets into spin conduits[9] and femtosecond laser excitations can generate superdiffusive spin currents,[10] which were shown to manipulate, for instance, domain wall profiles on ultrafast time scales.[11] The most widely used approach to date is nonlocal spin injection in a lateral spin valve [see Fig. 1(a)]. In this configuration, two ferromagnetic elements are connected by a nonmagnetic spin current conduit. By injecting a combined spin and charge current from one ferromagnet (in our case, FM1 at the bottom) into the paramagnetic spin current conduit (SCC), a spin accumulation is generated at the interface between the ferromagnet and the SCC, and this accumulation diffuses as a pure diffusive spin current in all directions, including along the SCC towards the top ferromagnet FM2.[12–14] At the interface between the SCC and FM2, the spin current is absorbed into the ferromagnet due to the low resistance of the ohmic contact between the SCC and FM2 leading to a low spin resistance of the ferromagnet.[15]

This absorbed spin current then exerts a torque on the magnetization in the absorbing ferromagnet. It has been shown that the absorbed spin current can reverse the magnetization of a small disk.[16] We demonstrated a high efficiency for domain wall motion,[17] as the spins in the spin current exhibit a large angle with respect to the magnetization direction in the small domain wall volume where they are absorbed, thereby exerting a large torque. This can lead to an efficiency that can be orders of magnitude larger than for combined spin and charge currents flowing in the ferromagnet.[17] Of course the domain wall motion using pure diffusive spin currents can only be induced while the domain wall is (at least partially) underneath the spin conduit because the spin-diffusion length in permalloy (Py) is of the order of a few nm.[18] Previously, we detected pure spin current-assisted depinning of a domain wall from a position underneath the SCC using a local-detection scheme based on the anisotropic magnetoresistance (AMR) in the ferromagnet.[17] While a very high spin transfer efficiency was found, this measurement was only able to detect a displacement of the domain wall from the area below the SCC to the outside area between the SCC and one of the adjacent contacts. This is due to the measurement scheme, where we probed the resistance of the FM area between the SCC and an adjacent contact and this resistance only changes if the wall moves into this area and is no longer underneath the SCC. Thus, such a measurement would not be able to detect a motion of the domain wall underneath the spin conduit as needed to demonstrate pure spin current-induced motion. Such pure

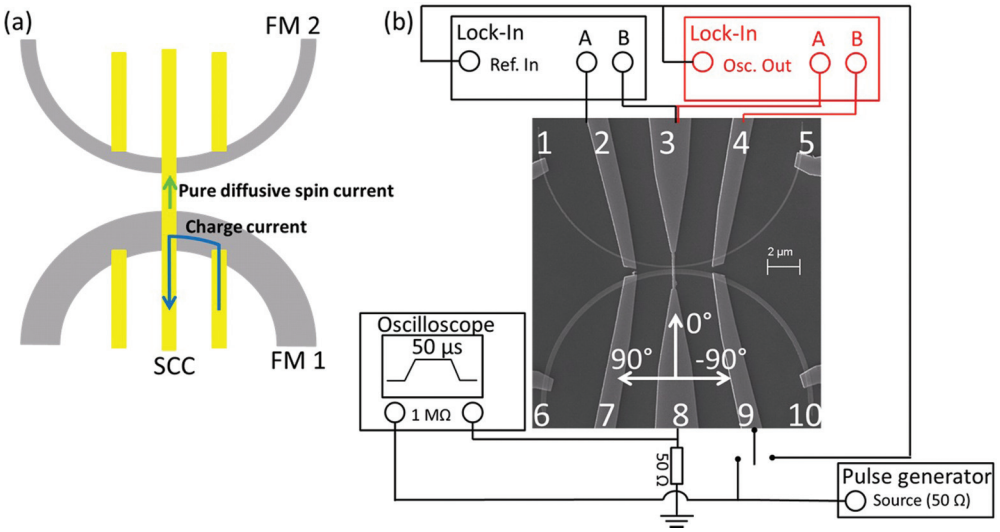

FIG. 1. (Color online) (a) Schematic depiction of a nonlocal spin valve consisting of two permalloy (Py) half rings [FM2 (top) and FM1 (bottom)] and a nonmagnetic copper spin current conduit (SCC) connecting both. (b) Scanning electron microscopy (SEM) image of a nonlocal spin valve device. The connections for the nonlocal resistance detection as well as the pulse injection are shown schematically with the numbered contacts.

spin current-induced domain wall motion and the related efficiency for this process are exactly the imperative pieces of information for any future device employing switching based on pure diffusive spin current-induced domain wall motion. To this end, we need to be able to detect the motion of the domain wall underneath the SCC. Unfortunately, the usual nonlocal spin valve measurements detect simply the effective magnetization direction underneath the SCC, from which it is not straightforward to detect whether the domain wall moves underneath the contact. However, upon closer inspection, the common simplification of assuming the magnetization below the spin conduit to be uniform leading to easily interpretable signals as one measures the voltage between the spin conduit and a contact on one side of the SCC, is only an approximation. In particular, one can measure the signal between the SCC and contacts on either side of the spin conduit; here some asymmetry can be anticipated since one does not probe the same part of the interface between the spin conduit and the ferromagnet. By measuring concurrently on both sides of the spin conduit, different parts of the SCC/FM interface will be detected, which would allow for a detection of the magnetization and thus the domain wall position locally underneath the spin conduit. This assumes that the spin current is not absorbed in a single small area of the interface, but rather that the interface exhibits a homogeneous spin resistance. There has been a debate as to what extent the spin currents are injected and absorbed at "hot spots" of the interface where particularly low spin resistances are present or whether a homogeneous injection and absorption is taking place. Note that in the case of hot spots, one would expect that the signals measured for contacts on both sides of the spin conduit would be identical, so such measurements also allow one to determine whether hot spots dominate the spin transport across the interface.

In this paper, we investigate the displacement of a transverse domain wall by a pure diffusive spin current in a nonlocal spin valve structure by monitoring the nonlocal spin resistance for multiple contacts. We can detect the motion of a domain wall underneath the spin conduit and we find that we can displace a domain wall at zero external magnetic field with spin currents $<10^{10}$ A/m^2, i.e., two orders of magnitude smaller than for conventional current-induced domain wall motion by combined spin and charge currents along the FM.

Nanostructures have been fabricated with a lateral spin valve geometry as shown in Fig. 1(a) by electron beam lithography and thin-film deposition of Py and copper. First, the two Py half-ring elements shown in Fig. 1 were deposited with a thickness of 30 nm and a width of 100 and 300 nm for the top (FM2) and bottom (FM1) half ring, respectively. As previously determined, in the narrower half ring, the transverse wall spin structure prevails, whereas in the wider half ring, a vortex wall is the stable configuration.[17,19] Second, *in situ* ion milling was used to clean the interface and then 90 nm copper (Cu) as the nonmagnetic material was deposited. On top of the Cu layers, Au was deposited to prevent oxidation. The width of this central Cu/Au SCC is 100 nm. Multiple samples with edge-to-edge distances between 100 and 300 nm as determined from SEM images were fabricated to determine the key spin transport properties. We did not use tunnel barriers at the ferromagnetic-spin conduit interfaces, even though large nonlocal resistances can be measured when using such tunnel barriers,[20,21] since they strongly limit the charge current that can be injected. Rather, our clean transparent interfaces allow for maximizing the injected charge current, and thus the spin current.

Transport measurements were carried out in a cryostat at 4.2 K using a dual lock-in technique with a current of 100 μA (current densities $<10^{11}$ A/m^2), as shown schematically in Fig. 1(a). We connect two lock-in amplifiers that concurrently monitor the nonlocal spin signals between the SCC [contact 3; see Fig. 1(b)] and the adjacent contacts to the left (2) and right (4), while injecting the current between contacts 8 and 9 by using a switch to connect contact 9 to the lock-in output.

With this measurement scheme, we have only high impedance (>10 MΩ) contacts connected to the top half ring, thereby ensuring that no charge current flows along the SCC and that all changes of the magnetization direction are induced by the pure spin current. In our setup, we use an in-plane rotatable external magnetic field to position domain walls.

We first determine the spin transport properties in our sample by using the standard approach laid out in Refs. 22 and 23 and previously used to determine the pure spin current density.[17] We measure the nonlocal resistance change for parallel and antiparallel alignment of the two ferromagnetic half rings for different samples and use the following formula:[17]

$$\Delta V_{NL}(d) = \frac{\alpha_F^2 I_C R_{S,F1} R_{S,F2} R_{S,N}}{\exp\left(\frac{d}{\lambda_N}\right)[R_{S,N}(R_{S,F1}+R_{S,F2})+2R_{S,F1}R_{S,F2}]+R_{S,N}^2\sinh\left(\frac{d}{\lambda_N}\right)}, \quad (1)$$

with $\Delta V_{NL}(d)$ being the difference in the nonlocal spin voltage between a parallel and antiparallel magnetic configuration. Here, d is the center to center distance between both FMs, α_F is the spin polarization in the FM, and $R_{S,i}$ is the spin resistance with $R_{S,i} = 2\rho_i\lambda_i/[S(1-\alpha_i^2)]$, where ρ_i is the resistivity, λ_i is the spin-diffusion length of the specific material, and S is the cross-sectional area. The spin current at the second interface is then given by $I_S(d) = \Delta V_{NL}(d)/(\alpha_F R_{S,F2})$ and the measured nonlocal spin resistance change is defined as $\Delta R_{NL} = \Delta V_{NL}/I_C$.

In Fig. 2(a), we show the results of the nonlocal measurements with spin signal amplitudes up to 1.5 mΩ (red and black up-triangle symbols), which are about ten time larger than in our previous samples[17] due to the optimized geometry and deposition conditions. From the fit of the signals for samples with different spacing to Eq. (1), we determine the spin-diffusion length in the Cu at 4 K to be $\lambda_N = \lambda_{Cu} = 350 \pm 40$ nm and the effective spin polarization to be $31 \pm 3\%$. The larger spin-diffusion length as compared with our previous finding[17] can be attributed to the two-times-larger thickness of the Cu, which leads to reduced surface scattering. Both values are in line with previous findings of many other groups; a systematic study was, for instance, carried out in Ref. 24. We note that the temperature dependence of our nonlocal spin signals exhibits a peak at 40 K, which was previously observed for Cu spin conduits and has been explained by the interplay of surface and bulk scattering.[25]

Having established the spin transport properties, we have all of the necessary ingredients to calculate the spin currents and study the domain wall positions and displacements. In the following, we focus on a sample with the minimum edge-to-edge spacing (100 nm) and we carry out the measurements at 4 K.

In order to be able to detect domain wall motion underneath the spin conduit, we first need to determine whether the spin absorption is homogeneous or whether hot spots dominate. Comparing the size of the signals for the measurement with the current injection between contacts 8 and 9 and the voltage measurements between contacts 2 and 3 (black up-triangles) as well as contacts 3 and 4 (red up-triangles), we see that the signal amplitudes are different, which already points to the fact that hot spots do not dominate the spin absorption, but rather the signal measured between contacts 2 and 3 results from spin absorption at a different part of the SCC-FM2 interface than the signal measured between contacts 3 and 4. So this means that by measuring at a contact to the left (signal between contacts 2 and 3), we probe the spin absorption of the left part of the interface between the SCC and FM2, while measuring between contacts 3 and 4, we probe the spin absorption of the right part of the interface. We can even obtain a rough estimate of the effective average distance difference between spin injection and spin absorption by entering the values for the measured nonlocal spin resistance into Eq. (1) and we obtain 60 nm. This is in line with a rough calculation of the geometrical distance: If we assume that the injection takes place close to the right edge of the interface between the spin current conduit SCC and FM1, and that the spin absorption takes place at the right and left edges of the interfaces between the SCC and FM2, we can calculate the difference in distance between the injection and the two absorption points and find 40 nm. This difference in the signal amplitude clearly points to a homogeneous spin current absorption, which one would expect for our clean transparent contacts. For tunneling contacts though, this might not hold, as hot spots where the tunnel barrier is slightly thinner can easily be present in these less robust systems.

Next we determine the magnetic properties of the samples, in particular the domain wall locations, as we need to position them underneath the spin conduit to realize the spin current-induced displacement measurements. To this end, we carry out local measurements (current between contacts 1 and 5 and voltage probed between contacts 2 and 3 or 3 and 4). If a domain wall is located between the voltage contacts, the resistance is lower because of the AMR contribution of the domain wall spin structure. We can thus precisely position the domain walls by applying fields along the appropriate direction and subsequently relaxing the field back to zero, at which point the domain wall will form at the corresponding angular position of the ring structure.

In Fig. 2(j), we show the results of these measurements for FM2. For angles between -10° and -1°, we find a low resistance state measured between contacts 2 and 3 [black signal in Fig. 2(j)]. This means the domain wall in FM2 is to the left of contact 3 [sketched in Figs. 2(c) and 2(d) and corresponding to the red levels I and II in Fig. 2(b), as discussed later]. For angles between -1° and 1.4°, the domain wall is partly underneath the center contact 3 [sketched in Fig. 2(e) and corresponding to the red level III in Fig. 2(b)]. This corresponds to an intermediate resistance state measured between contacts 2 and 3 [black signal in Fig. 2(j)] as the domain wall is partly between contacts 2 and 3 and thus reduces

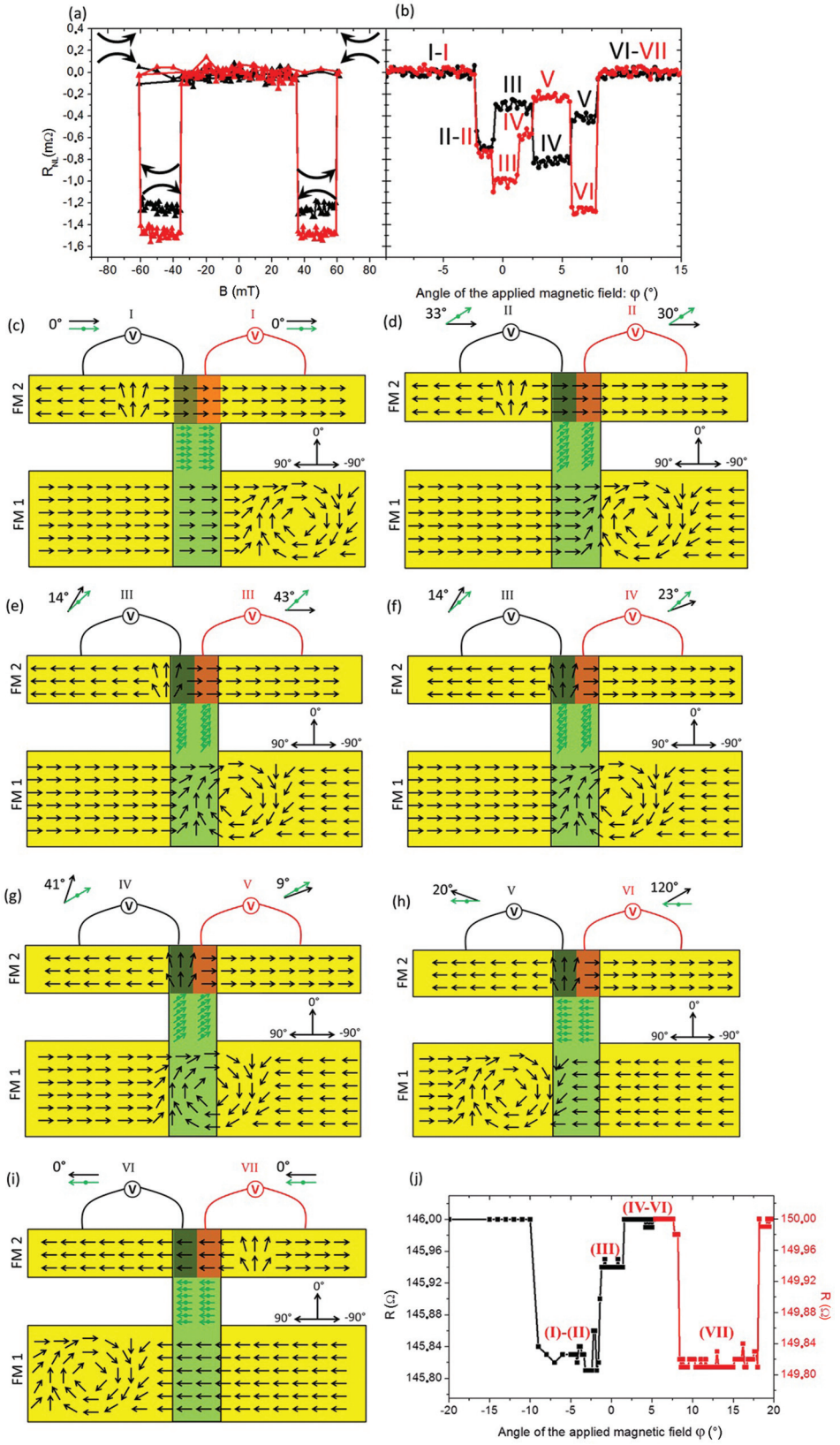

FIG. 2. (Color online) (a) Nonlocal measurements showing the nonlocal resistance measured between contacts 2 and 3 (black) and contacts 3 and 4 (red) as the field is swept along 90°. The arrows indicate the directions of the magnetization in the two half rings, showing that the wider half ring switches at lower fields as expected, resulting in low nonlocal resistance states with antiparallel alignment of the half rings and high resistance states for parallel alignment. (b) Measurement of the nonlocal resistance between contacts 2 and 3 (black) and contacts 3 and 4 (red) as a function of the field direction that positions the domain walls (disc symbols). The different domain wall positions leading to different values of the nonlocal resistances are indicated by roman numerals. (c)–(i) Schematic representations of the different domain wall positions deduced from a combination of the measured local and nonlocal signals. The direction of the spins in the spin current is shown by the green arrows in the spin conduit. The average angle between the spins in the spin current and the magnetization in the two SCC-FM2 interface areas as deduced from the nonlocal resistance levels is shown by the black and green arrows and the value of the angle shown above each schematic. In (c)–(i), the approximate regions that are probed by the two measured signals are indicated by the red and black shaded areas. In (j), we show the local voltage measured between contacts 2 and 3 (black) and contacts 3 and 4 (red) when injecting the current between contacts 1 and 5. The signal changes result from the different AMR when the spin structure changes between the contacts when the domain wall is moved.

the resistance less than in the case where it is fully between contacts 2 and 3 (for angles $<-1.5°$). For angles between 1.4° and 8°, the domain wall is underneath the center contact [sketched in Figs. 2(f)–2(h) and corresponding to the red levels IV–VI in Fig. 2(b)]. This corresponds to the high resistance state measured between both contacts 2 and 3 [black signal in Fig. 2(j)] and between 3 and 4 [red signal in Fig. 2(j)] as the domain wall is neither between contacts 2 and 3, nor between contacts 3 and 4. Finally, for angles above 8°, the domain wall is to the right of contact 3 [sketched in Fig. 2(i)

and corresponding to the red level VII in Fig. 2(b)]. This corresponds to the low resistance state measured between contacts 3 and 4 [red signal in Fig. 2(j)] as the domain wall is fully located between contacts 3 and 4 and thus reduces the resistance of this part of the wire. Note that for angles $<-10^\circ$ and $>18^\circ$, the domain wall is outside the probed area between contacts 2 and 4.

So from these measurements we know that the transverse domain wall in FM2 is located (at least partially) in the area underneath the SCC for applied field angles between -1° and $+8^\circ$. Analogously, we find that the vortex domain wall in FM1 enters the contact area at -2° and also leaves completely for fields also at $+8^\circ$.

In addition to this simple AMR measurement, we next use the new dual nonlocal measurements (current injected between contacts 8 and 9) to obtain more insight into the detailed domain wall positions as shown in Fig. 2(b), which we discuss now. The first surprising observation is that the signals measured between the contact on the left (black symbols, contacts 2 and 3) and on the right (red symbols, contacts 3 and 4) are very different, demonstrating that indeed the two signals probe different parts of the interface between the SCC and FM2, ruling out hot spots for the spin current absorption. Second, we observe clear distinct jumps in the signal as a function of the applied field direction, showing that there are a finite number of distinct positions for the two domain walls in FM1 and FM2 as a direct consequence of the potential landscape variations, as previously observed.[26] In order to understand the signals and deduce the domain wall positions, we need to understand what the different nonlocal resistance levels mean. The nonlocal voltage measured between contacts 2 and 3 is a measure of the difference in the chemical potential of the spin current from the spin conduit and the average magnetization in approximately the left half of the interface area between the SCC and FM2, assuming homogeneous current absorption. For contacts 3 and 4, the right half of the interface area is probed. Both of these areas are, respectively, indicated by the red and black shaded areas in Fig. 2(c). By comparing Figs. 2(a) and 2(b), we can see that in Fig. 2(a) the I-black–I-red and VI-black–VII-red levels correspond to parallel alignment of the magnetization in both half rings. Furthermore, the VI-red level is close to the lower level of the red curve in Fig. 2(a), showing that it corresponds nearly to an antiparallel alignment of the spins in the spin current (resulting from the magnetization at the injection area of the SCC-FM1 interface) and the right part of the SCC-FM2 interface area. Scaling the two levels (parallel and antiparallel alignment) between -1 and 1, the level directly corresponds to $\cos(\theta)$, with θ the angle between the spins in the spin current (and thus as a first approximation the magnetization in the right half of the SCC-FM1 interface when the current is injected between contacts 8 and 9) and the average magnetization in the corresponding SCC-FM2 interface area.

As we increase the direction of the field to position the domain wall along -2°, the signals of the left and right SCC-FM2 contact area change identically. This means that the magnetization in the total SCC-FM2 interface area is still homogeneous (the magnetization in both halves is identical), but the injector magnetization at the interface SCC-FM1 has changed. This can be explained by the larger vortex domain wall moving into this area, as shown schematically in Fig. 2(d), leading to an increase in the angle between the spins in the spin current and the magnetization at the SCC-FM2 interface. This is further corroborated by the locally measured resistance values between contacts 2 and 3, which shows that the transverse domain wall is still fully in the area between the contacts and has not entered the SCC-FM2 interface area. At -0.8°, a different behavior for the two non-local signals is observed. The signal between contacts 2 and 3 (III-black) increases, indicating that the magnetization in the left area is nearly parallel to the spins in the spin current, while the magnetization in the right area (III-red) becomes more antiparallel. This different behavior shows that the transverse domain wall has started to move into the left part of the SCC-FM2 contact area, while the vortex wall moves slightly further into the SCC-FM1 area, thereby changing the direction of the spins in the spin current. This is depicted schematically in Fig. 2(e). At $+1^\circ$, only the signal between contacts 3 and 4 (IV-red) changes significantly. This behavior can be understood by supposing that the transverse wall extends further towards the right of the SCC-FM2 contact area [Fig. 2(f)], but that the magnetization of the right part remains unchanged. At $+2^\circ$, the signal between contacts 2 and 3 (IV-black) shows an increase of the angle between the spins of the spin current and the magnetization of the left area of the SCC-FM2 interface, while the signal between contacts 3 and 4 (V-red) indicates a more parallel alignment. This can be explained by the vortex wall moving further into the SCC-FM1 interface area, as shown in Fig. 2(g). At $+6^\circ$, the signal changes reverse, showing that the left SCC-FM2 area (V-black) becomes more parallel, whereas in the right SCC-FM2 area (VI-red), the magnetization becomes nearly completely antiparallel to the injected spin current. This corresponds to the configuration in Fig. 2(h), where the vortex wall has moved nearly out of the SCC-FM1 contact area and has thereby reversed the SCC-FM1 interface area. As the right half of the SCC-FM2 interface area still has its original magnetization direction, this corresponds to a (nearly) antiparallel alignment. Finally, at $+8^\circ$, the transverse wall moves across the SCC-FM2 interface area, and the complete parallel alignment, with both the magnetization in the SCC-FM1 and the SCC-FM2 interface areas reversed, is obtained as shown in Fig. 2(i). Note that from the geometry and the field direction, the spin structure of the transverse wall in FM2 is set, whereas the vortex wall in FM1 could have a clockwise (as shown here) or a counterclockwise chirality. However, it is clear that the measured nonlocal signals can only be explained by a clockwise vortex wall moving across the SCC-FM1 interface area, which demonstrates the power of our method that allows us to even determine the chirality (in-plane sense of rotation) of the vortex wall in the wider half ring FM1.

Now we use this tool developed here that allows us to probe the displacement of domain walls even underneath the spin conduit to set the desired spin configuration and to probe the behavior when injecting pure spin currents. To this end, we initialize the magnetization configuration with a field along $+7^\circ$ to obtain the configuration depicted in Fig. 2(h), where the spins in the injected spin current point along the $+90^\circ$ direction and are thus perpendicular to the magnetization at the center of the transverse wall (0°). Next we follow the protocol

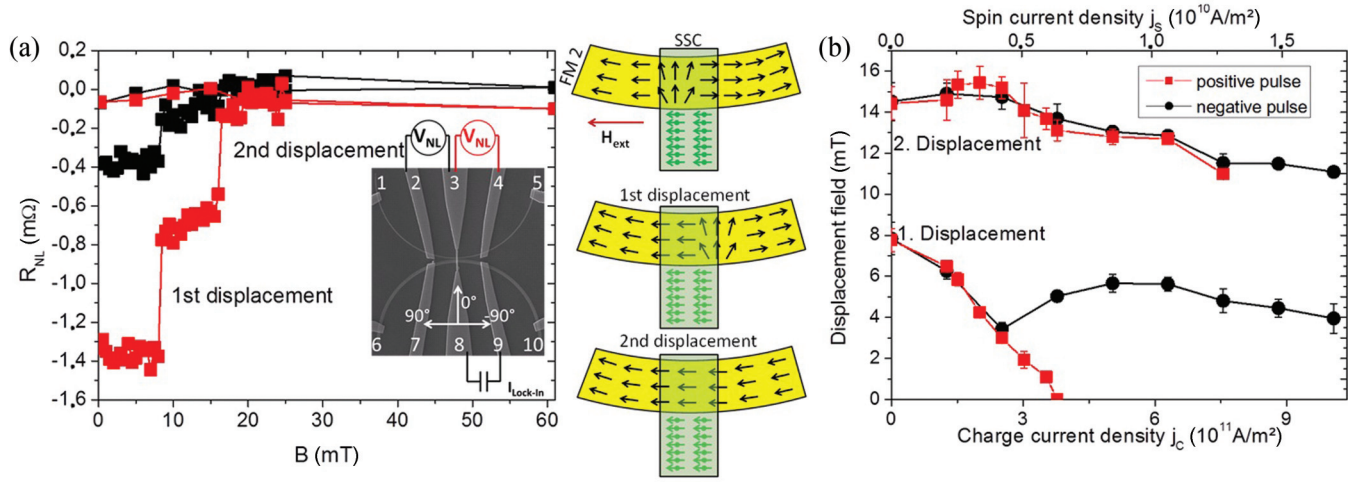

FIG. 3. (Color online) (a) Nonlocal signal between contacts 2 and 3 (black discs) as well as contacts 3 and 4 (red discs) as a field is applied along $+90^\circ$ to a domain wall located underneath the SCC-FM2 interface area. Two switching events are discernible, at 8 and 15 mT. The inset shows the measurement configuration for both signals. To the right, the initial spin configuration and the first and second domain wall displacement events are shown schematically. (b) Domain wall displacement fields as a function of injected current density (charge current shown on the bottom x-axis and corresponding calculated spin current shown on the top x-axis). The different pulse polarities show that positive pulses support the wall motion, while negative pulses impede it.

established in Ref. 17, where we apply a perpendicular field H_{ext} along $+90^\circ$ and inject the spin current as 50 μs long pulses by connecting contact 9 to the output of the pulse generator. Two effects will occur: (i) Heating might lead to a reduction of the field needed to move the domain wall and this should be independent of the pulse polarity. (ii) For one pulse current polarity, the spin current will support the motion, leading to a reduction in the external field necessary to displace the wall, while for the opposite polarity, the spin current will impede the motion and thus will not reduce the field. In Fig. 3(a), we first show the displacement of the transverse wall probed by the dual nonlocal resistance measurement. At zero field, both signals (between contacts 2 and 3 as well as contacts 3 and 4) start in the levels expected for a transverse wall located underneath the SCC-FM2 interface area [Fig. 2(h)]. At 8 mT, both signals show a jump to a more parallel alignment state, demonstrating that the transverse wall has been displaced underneath the spin conduit from the left half to the right half, as shown schematically in Fig. 3(a). From the levels, it is clear that the wall has moved out of the left part of the SCC-FM2 interface area and is now located at the very right edge of the SCC-FM2 interface area where only a small spin current will act. At 15 mT, the wall completely moves out of the SCC-FM2 contact area ("2nd displacement"). Note that as the vortex wall in FM1 already left the relevant contact area, any further motion of the wall will not further change the orientation of the injected spin current.

In Fig. 3(b), we now plot the displacement fields for the two detected displacements as a function of the injected current density for both current polarities. We calculated the spin current density using the determined spin-polarization and spin-diffusion lengths.[17] We start by discussing the first displacement starting at around 8 mT, which corresponds to a position below the SCC-FM2 interface, where a large spin current acts on the transverse wall. We see that for small current densities, there is some reduction of the displacement field for both current polarities due to heating, as previously observed.[27] For larger current densities, the depinning fields are further reduced for positive spin current polarities (supporting the wall motion), while this is not the case for negative spin current polarities. Next we determine the efficiency as used previously, namely, the field-current equivalence as described in Ref. 28, and find $\epsilon = (1.30 \pm 0.08) \times 10^{-12}$ Tm^2/A, which is more than one order of magnitude larger than previously found for nonlocal spin valves[17] and two to three orders of magnitude larger than the values found for combined spin and charge currents injected along ferromagnetic wires.[19] While for the torques acting there is no strict field-current equivalence, this value allows for comparison to previous work nonetheless. In fact, even the charge-current density used is an order of magnitude lower than those observed for currents injected along ferromagnetic wires.

Finally, we also look at the second displacement for the domain wall from the edge of the SCC-FM2 interface area. Here we see that there is only a small change, probably due to heating. Only for the largest current densities do the positive pulses that support the motion show a slightly larger reduction of the displacement field than negative currents. This is expected because at the edge of the conduit the spin current only acts on part of the domain wall. Furthermore, the fact that the change is small also shows that the observed effect cannot originate from Oersted fields. Oersted field effects should be nearly identical for the two domain wall displacements and thus the changes in the displacement field with current density should also be nearly identical, while the region where the spin current acts is very localized: the effect depends strongly on the position of the domain wall with respect to the SCC-FM2 interface and falls off extremely rapidly (over a few nm) outside this area.

In summary, we have studied pure spin current-induced domain wall motion using a specially designed nonlocal detection scheme that allows us to probe precisely the domain wall motion underneath the spin conduit. We find that our method allows us to ascertain the spin configurations in the injector

and the detector ferromagnets, including the detailed domain wall positions. By injecting pure diffusive spin currents, we are able to displace a transverse domain wall without any externally applied fields, demonstrating that these currents can manipulate domain walls at low spin current densities of $<10^{10}$ A/m^2. We find that this originates from the efficiency in our optimized device $[(1{,}30 \pm 0{,}08) \times 10^{-12}$ Tm^2/A]. This high efficiency means that even though only a small fraction of the spin current generated arrives at the domain wall, the critical charge-current density for wall displacement is still lower than previously observed for Py.

These findings open new avenues for devices: With the large changes in the nonlocal signal (and no background signal is expected since there are no charge-current magnetoresistance effects during read-out in the nonlocal geometry), one can envisage the generation of a 1 bit memory similar to the magnetoresistive random-access memory (MRAM) design put forward by Numata *et al.*[29] Furthermore, using the recently established principle of domain wall automotion,[30] one can judiciously design the geometry to displace the domain wall underneath the SCC to a high-energy position from which it moves by automotion to the next SCC. This can be achieved, for instance, by periodically varying the width of a magnetic wire and having SCCs attached to it periodically.

This work was funded by the German Ministry for Education and Science (BMBF), the DFG, the Graduate School of Excellence Material Science in Mainz (Project No. GSC 266), the EU 7th Framework Programme IFOX (Program No. NMP3-LA-2010 246102), MAGWIRE (Program No. FP7-ICT-2009-5 257707), MoQuaS (Program No. FP7-ICT-2013-10 610449), WALL (Program No. FP7-PEOPLE-2013-ITN 608031), the European Research Council through the Starting Independent Researcher Grant MASPIC (Grant No. ERC-2007-StG 208162), the Research Center Complex Materials (COMATT), and the Agence Nationale de la Recherche (ANR-10-BLANC-SPINHALL). The devices were fabricated at the Plateforme Technologique Amont in Grenoble.

*Klaeui@uni-mainz.de

[1] S. S. P. Parkin, M. Hayashi, and L. Thomas, Science **320**, 190 (2008).
[2] L. Berger, J. Appl. Phys. **55**, 1954 (1984).
[3] J. C. Slonczewski, J. Magn. Magn. Mater. **159**, L1 (1996).
[4] A. Yamaguchi, T. Ono, S. Nasu, K. Miyake, K. Mibu, and T. Shinjo, Phys. Rev. Lett. **92**, 077205 (2004).
[5] M. Kläui, C. A. F. Vaz, J. A. C. Bland, W. Wernsdorfer, G. Faini, E. Cambril, L. J. Heyderman, F. Nolting, and U. Rüdiger, Phys. Rev. Lett. **94**, 106601 (2005).
[6] J. Grollier, P. Boulenc, V. Cros, A. Hamzic, A. Vaures, A. Fert, and G. Faini, Appl. Phys. Lett. **83**, 509 (2003).
[7] F. Junginger, M. Kläui, D. Backes, U. Rüdiger, T. Kasama, R. E. Dunin-Borkowski, L. J. Heyderman, C. A. F. Vaz, and J. A. C. Bland, Appl. Phys. Lett. **90**, 132506 (2007).
[8] J. Sinova and I. Zutic, Nat. Mater. **11**, 368 (2012).
[9] Y. Tserkovnyak, A. Brataas, G. E. W. Bauer, and B. I. Halperin, Rev. Mod. Phys. **77**, 1375 (2005).
[10] M. Battiato, K. Carva, and P. M. Oppeneer, Phys. Rev. Lett. **105**, 027203 (2010).
[11] B. Pfau, S. Schaffert, L. Müller, C. Gutt, A. Al-Shemmary, F. Büttner, R. Delaunay, S. Düsterer, S. Flewett, R. Frömter, J. Geilhufe, E. Guehrs, C. M. Günther, R. Hawaldar, M. Hille, N. Jaouen, A. Kobs, K. Li, J. Mohanty, H. Redlin, W. F. Schlotter, D. Stickler, R. Treusch, B. Vodungbo, M. Kläui, H. P. Oepen, J. Lüning, G. Grübel, and S. Eisebitt, Nat. Comm. **3**, 1100 (2012).
[12] S. O. Valenzuela and M. Tinkham, Nature (London) **442**, 176 (2006).
[13] F. J. Jedema, A. T. Filip, and B. J. van Wees, Nature (London) **410**, 345 (2001).
[14] M. Johnson and R. H. Silsbee, Phys. Rev. B **37**, 5326 (1988).
[15] T. Kimura, J. Hamrle, Y. Otani, K. Tsukagoshi, and Y. Aoyagi, Appl. Phys. Lett. **85**, 3795 (2004).
[16] T. Yang, T. Kimura, and Y. Otani, Nat. Phys. **4**, 851 (2008).
[17] D. Ilgaz, J. Nievendick, L. Heyne, D. Backes, J. Rhensius, T. A. Moore, M. A. Nino, A. Locatelli, T. O. Mentes, A. v. Schmidsfeld, A. v. Bieren, S. Krzyk, L. J. Heyderman, and M. Kläui, Phys. Rev. Lett. **105**, 076601 (2010).
[18] S. Dubois, L. Piraux, J. M. George, K. Ounadjela, J. L. Duvail, and A. Fert, Phys. Rev. B **60**, 477 (1999).
[19] M. Laufenberg, D. Backes, W. Buhrer, D. Bedau, M. Kläui, U. Rüdiger, C. A. F. Vaz, J. A. C. Bland, L. J. Heyderman, F. Nolting, S. Cherifi, A. Locatelli, R. Belkhou, S. Heun, and E. Bauer, Appl. Phys. Lett. **88**, 232507 (2006).
[20] S. O. Valenzuela and M. Tinkham, Appl. Phys. Lett. **85**, 5914 (2004).
[21] A. Vogel, J. Wulfhorst, and G. Meier, Appl. Phys. Lett. **94**, 122510 (2009).
[22] S. Takahashi and S. Maekawa, Phys. Rev. B **67**, 052409 (2003).
[23] T. Kimura, Y. Otani, and J. Hamrle, Phys. Rev. B **73**, 132405 (2006).
[24] F. J. Jedema, M. S. Nijboer, A. T. Filip, and B. J. van Wees, Phys. Rev. B **67**, 085319 (2003).
[25] T. Kimura, T. Sato, and Y. Otani, Phys. Rev. Lett. **100**, 066602 (2008).
[26] X. Jiang, L. Thomas, R. Moriya, and S. S. P. Parkin, Nano Lett. **11**, 96 (2011).
[27] M. Laufenberg, W. Bührer, D. Bedau, P. E. Melchy, M. Kläui, L. Vila, G. Faini, C. A. F. Vaz, J. A. C. Bland, and U. Rüdiger, Phys. Rev. Lett. **97**, 046602 (2006).
[28] J. Heinen, O. Boulle, K. Rousseau, G. Malinowski, M. Kläui, H. J. M. Swagten, B. Koopmans, C. Ulysse, and G. Faini, Appl. Phys. Lett. **96**, 202510 (2010).
[29] H. Numata, T. Suzuki, N. Ohshima, S. Fukami, K. Nagahara, N. Ishiwata, and N. Kasai, IEEE Symposium on VLSI Technology, Digest of Technical Papers 232 (2007).
[30] J.-Y. Chauleau, R. Weil, A. Thiaville, and J. Miltat, Phys. Rev. B **82**, 214414 (2010).